Journal of Luminescence 206 (2019) 227–233

Contents lists available at ScienceDirect

Journal of Luminescence

journal homepage: www.elsevier.com/locate/jlumin

Tunable luminescence of $Na_3YSi_3O_9:Ce^{3+}$, Mn^{2+} *via* efficient energy transfer for white LEDs

Fei Wang[a], Ye Jin[a,*], Yongfu Liu[b,*], Liangliang Zhang[c], Rui Dong[b], Jiahua Zhang[c,*]

[a] School of Science, Chongqing University of Technology, 69 Hongguang Street, Chongqing 400054, China
[b] Ningbo Institute of Materials Technology and Engineering, Chinese Academy of Sciences, Ningbo 315201,China
[c] State Key Laboratory of Luminescence and Applications, Changchun Institute of Optics, Fine Mechanics and Physics, Chinese Academy of Sciences, 3888 Eastern South Lake Road, Changchun 130033, China

ARTICLE INFO

Keywords:
$Na_3YSi_3O_9:Ce^{3+}$, Mn^{2+}
Energy transfer
Phosphor
White LED

ABSTRACT

Ce^{3+} and Mn^{2+} co-doped $Na_3YSi_3O_9$ (NYS) phosphors with tunable emission were prepared *via* a high-temperature solid-state reaction. Under 320-nm excitation, $Na_3YSi_3O_9:Ce^{3+}$, Mn^{2+} exhibits two broad emission bands from 340 to 590 nm and from 525 to 700 nm, ascribed to the 5d-4f transition of Ce^{3+} and the $^4T_1(^4G)$-$^6A_1(^6S)$ spin-forbidden transition of Mn^{2+}, respectively. Energy transfer from Ce^{3+} to Mn^{2+} through a dipole-dipole interaction was explained based on the luminescence spectra and fluorescence decay curves. The critical distance of energy transfer was calculated to be 12.836 Å, and the energy transfer efficiency reached as high as 91.9%. Temperature-dependent luminescence was studied, and the corresponding activation energy Δ E was calculated to be 0.221 eV. Tunable luminescence from blue to orange was realized utilizing the energy transfer from Ce^{3+} to Mn^{2+}. A warm white light with CIE chromaticity coordinates of (0.3627, 0.2855) and color temperature of 3612 K was achieved. These results indicate that NYS:Ce^{3+}, Mn^{2+} may have potential application in UV-pumped white-light-emitting diodes.

1. Introduction

White light-emitting diodes (WLEDs) have attracted extensive interest due to their merits of long lifetime, energy saving qualities, high luminous efficiency, environmentally friendly characteristics and so on [1–7]. WLEDs, generated by the combination of a blue InGaN chip and the yellow-emitting $Y_3Al_5O_{12}:Ce^{3+}$ (YAG:Ce^{3+}) phosphors, usually offers an unsatisfactory correlated color temperature (CCT, usually higher than 4500 K) and a low color rendering indexes (CRI, less than 80) due to the deficient red light for general illumination [8]. In order to overcome these disadvantages, WLEDs are fabricated by using ultraviolet (UV) LED chips coaching with red, green, and blue phosphors or a single-phase phosphor having red, green and blue emissions. It is of great interest to develop a single-phase phosphor because it has the advantages of low color aberration, excellent color rendering index, good color tone, and tenability of the CIE color coordinates and the CCT [9–12]. Single-phase phosphors are often color tunable through energy transfers from sensitizer to activator by co-doping right sensitizers and activators in the determined host. Several single-component white-light phosphors have been reported, such as $Ca_4Si_2O_7F_2:Eu^{2+}$, Mn^{2+} [12], $CaAl_2Si_2O_8:Eu^{2+}$, Mn^{2+} [13], $Sr_3Al_2O_5Cl_2:Ce^{3+}$, Eu^{2+} [14], $Ca_5(PO_4)_2SiO_4:Ce^{3+}/Tb^{3+}/Mn^{2+}$ [15], and so on [16,17].

Rare earth ion Ce^{3+} shows a high efficiency in many hosts due to the parity-allowed electric-dipole transition between the 4f ground states and 5d excited states. The emission can extend from UV to yellow region, depending on host lattices [18]. Due to the $^4T_1$–$^6A_1$ transition strongly affected by the strength of the crystal field, Mn^{2+} doped phosphors often emit a broad emission band ranging from 500 to 700 nm, from green (weak crystal field) to red (stronger crystal field) [12]. However, the Mn^{2+} ion is very difficult to be pumped because of its forbidden d-d electric dipole absorptions, resulting in a weak emission. Usually, Ce^{3+} is an efficient sensitizer to enhance the Mn^{2+} emission through energy transfers. Thus, a series of Ce^{3+}/Mn^{2+} co-doped phosphors have been reported [15,17].

As an important compound, silicate phosphors have been widely investigated because of their excellent physical, chemical and thermal stability and excellent weather-resistance than other compounds especial fluorides and sulfides [12,19–21]. The $Na_3YSi_3O_9$ (NYS) host has a mixed octahedral-tetrahedral framework, where the YO_6 octahedral structure is conjunct with SiO_4 tetrahedral structure. The octahedral-tetrahedral framework makes $Na_3YSi_3O_9$ more stable. It is a proper host for rare-earth ions-activated phosphors with high luminous efficiency

* Corresponding authors.
E-mail addresses: jinye@cqut.edu.cn (Y. Jin), liuyongfu@nimte.ac.cn (Y. Liu), zhangjh@ciomp.ac.cn (J. Zhang).

https://doi.org/10.1016/j.jlumin.2018.10.033
Received 15 June 2018; Received in revised form 2 September 2018; Accepted 8 October 2018
Available online 12 October 2018

based on the closed shell configuration of s^2p^6 of the Y^{3+} cation [22,23]. To the best of our knowledge, there have been no reports regarding the investigation of NYS:Ce^{3+}, Mn^{2+}. Herein, NYS:Ce^{3+}, Mn^{2+} was synthesized by a high-temperature solid-state reaction. The luminescence properties, the energy transfer mechanism, luminescence decay curves, and thermal stability were investigated systematically. The correlated critical distance (Rc) of energy transfer, the energy transfer efficiency, the activation energy (Δ E) of thermal quenching, CIE color coordinates and CCT were calculated. All the results showed that NYS:Ce^{3+}, Mn^{2+} may have potential application as an UV-based WLEDs phosphor.

2. Experimental section

2.1. Materials and synthesis

The NYS:Ce^{3+}, Mn^{2+} samples were synthesized by a conventional high-temperature solid-state reaction. The detailed synthesized process and characterization of the samples can be found in our previous report [23]. The starting materials Na_2CO_3 (A.R.), SiO_2 (A.R.), Y_2O_3 (A.R.), $MnCO_3$ (A.R.) and CeO_2 (4 N) were weighed and all raw materials were mixed, and then grounded evenly in an agate mortar for 45 min. Finally, the mixture was put in an alumina crucible and continually fired at 1100 °C in a reducing atmosphere for 6 h. The products were cooled to room temperature in the furnace.

2.2. Measurements and characterization

The crystal structure determination of the as-prepared phosphors was performed by an X-ray diffraction (XRD) analysis using a Bruker-D8 powder diffractometer (XRD) with Cu K_α ($\lambda = 1.54078$ Å) radiation operating at 40 kV and 40 mA. The dates were collected over a 2θ range from 10° to 80°. The general structure analysis system (GSAS) program was used for structural refinement using the Rietveld method [24]. Room temperature photoluminescence emission (PL) and photoluminescence excitation (PLE) spectra were measured on a Hitachi F-4600 spectrophotometer with a 150 W Xe-arc lamp as the excitation lamp. The temperature-dependent luminescence properties were measured on the same spectrophotometer, which was combined with a self-made heating attachment and a computer-controlled electric furnace. The lifetimes were recorded on an FLS980 fluorescence spectrophotometer with a nanosecond flash nF920 as the excitation resource.

3. Results and discussion

3.1. Crystal structure

The XRD patterns of NYS:0.03Ce^{3+}, NYS:0.05Mn^{2+} and NYS:0.03Ce^{3+}, 0.05Mn^{2+} and the standard pattern of NYS (ICSD #20774) were given in Fig. 1(a). It can be found that all samples exhibit a single crystal phase and the doped Ce^{3+} and Mn^{2+} ions did not cause any notable impurities. Meanwhile, as Fig. 1(b) shows, the main diffraction peaks shift to the higher angle region when Ce^{3+} and Mn^{2+} ions are incorporated into the NYS host. In NYS, the effective ionic radii of Na^+ (CN = 6) is 1.02 Å, and the values are 0.88 Å and 0.26 Å for Y^{3+} (CN = 6) and Si^{4+} (CN = 4), respectively. The ionic radii of Ce^{3+} and Mn^{2+} are 1.01 Å and 0.83 Å (CN = 6), respectively. Therefore, it is practicable that Ce^{3+} ions substitute for the six-coordinated Na^+ site by comparing the values of effective ion radii. [23] Based on the percentage difference of the ion radii between the doped and substituted ions lower than 30%, it is supposed that Mn^{2+} ions substitute the sites of six-coordinated Na^+ and Y^{3+}. While from Fig. 5 later, the Ce^{3+} or Mn^{2+} emission redshift only affect by changing Ce^{3+} ions or Mn^{2+} ions itself. It means that the lattice environment around the doped ion is different. Furthermore, Mn^{2+} ion should locate on the Y^{3+} site. The right shift of the main diffraction peaks is shown in Fig. 1(b). The Rietveld structural refinement of NYS:0.03Ce^{3+}, 0.05Mn^{2+} was performed as shown in Fig. 2, and the refined parameters are listed in Table 1. $Na_3YSi_3O_9$:0.03Ce^{3+}, 0.05Mn^{2+} crystallizes into the orthorhombic system with a space group of P 21 21 21 (19), the lattice parameters were fitted to be $a = 15.2138(8)$ Å, $b = 15.1452(4)$ Å, $c = 15.0363(1)$ Å, $\alpha = \beta = \gamma = 90°$, $V = 3464.63(8)$ Å^3, and $Z = 16$. The accepted reliability factors of $\chi^2 = 1.948$, $R_{wp} = 6.44\%$ and $R_p = 5.07\%$ also indicate that doping Ce^{3+} and Mn^{2+} ions into NYS did not generate any impurity.

3.2. Luminescence properties of NYS:Ce^{3+}, Mn^{2+}

NYS:Ce^{3+} manifests a tunable luminescence dependent on Ce^{3+} concentrations and the selected excitation wavelengths [23]. The PL and PLE spectra of NYS:0.03Ce^{3+} are shown in Fig. 3(a). NYS:0.03Ce^{3+} has a broad excitation band ranging from 240 to 380 nm due to the 4f-5d transitions of Ce^{3+}. Upon 320 nm excitation, NYS:0.03Ce^{3+} gives rise to a blue emission band ranging from 340 to 590 nm with a peak at about 407 nm. The asymmetric emission band can be deconvoluted into two Gaussian curves centering at 23,283 cm^{-1} (429 nm) and 25,348 cm^{-1} (394 nm), as shown in Fig. 3(b). The energy difference is about 2065 cm^{-1}, which is attributed to the transitions from the lowest 5d excited state to the $^2F_{5/2}$ and $^2F_{7/2}$ ground states due to spin-orbit coupling [25]. The inset shows the emission intensity of NYS:Ce^{3+} as a function of the Ce^{3+} concentration and the optimum value of Ce^{3+} is 0.03 mol.

Since the d-d electric dipole absorption transitions are forbidden, Mn^{2+} ions are very difficult to be pumped and the emissions of Mn^{2+} are very week and hardly to be detected [12,26]. As a result, there was no emission was observed for $Na_3YSi_3O_9$:Mn^{2+}. Associating Mn^{2+} with sensitizers, such as Ce^{3+}, is a universal way to enhance the Mn^{2+} emission [27]. As shown in Fig. 4, when NYS:0.03Ce^{3+}, 0.03Mn^{2+} is excited by 320 nm, the PL spectrum displays a strong broad emission band from 525 to 700 nm in addition to the Ce^{3+} blue emission peaking at about 407 nm. The broadband peaking at 598 nm is consistent with the Mn^{2+} emission reported in many papers [11,12,28,29]. Therefore, it is reasonable to conclude that the broad emission band is ascribed to the $^4T_1(^4G)$-$^6A_1(^6S)$ spin-forbidden transition of Mn^{2+}. Moreover, the PLE spectrum of NYS:0.03Ce^{3+}, 0.03Mn^{2+} monitored at 598 nm has a profile similar to that monitored at 407 nm of the Ce^{3+} emission. Those results imply the energy transfer from Ce^{3+} to Mn^{2+}.

3.3. Energy transfer and emission red shift in NYS:Ce^{3+}, Mn^{2+}

In order to verify the energy transfer process, a series of $Na_3YSi_3O_9$:xCe^{3+}, yMn^{2+} phosphors were prepared. Fig. 5(a) and (b) show the PL spectra of NYS:0.03Ce^{3+}, yMn^{2+} (y = 0–0.11) and NYS:xCe^{3+}, 0.05Mn^{2+} (x = 0.01–0.05) excited at 320 nm. The emission intensity of Ce^{3+} decreases with the increase of Mn^{2+} contents, proving the presence of the energy transfer from Ce^{3+} to Mn^{2+} in NYS:Ce^{3+}, Mn^{2+}. Additionally, the decreases of Mn^{2+} emission intensity could be ascribed to the concentration quenching effect when $y > 0.07$. The concentration quenching can be attributed to the energy reabsorption among the nearest Ce^{3+} or Mn^{2+} ions [30]. Moreover, the PL spectra intensities of Ce^{3+} decrease with increasing Ce^{3+} content, while the emission of Mn^{2+} increases until x = 0.03 and then decrease, as illustrated in Fig. 5(b). The decline of Ce^{3+} emission and the increase of Mn^{2+} emission are ascribed to the energy transfer from Ce^{3+} to Mn^{2+}. The later decrease of Mn^{2+} emission is ascribed to the concentration quenching of Ce^{3+} as the concentration $x > 0.03$, which is consistent with the above consequence.

Additionally, an interesting redshift is concerned comparing the PL spectra of Ce^{3+} and Mn^{2+} in Fig. 5(a) and (b). The emission peaks of Mn^{2+} shift from 591 nm for y = 0.01–602 nm for y = 0.11 in NYS:0.03Ce^{3+}, yMn^{2+} and the peaks of Ce^{3+} have almost no shift. However, the emission peaks of Ce^{3+} redshift from 401 nm for

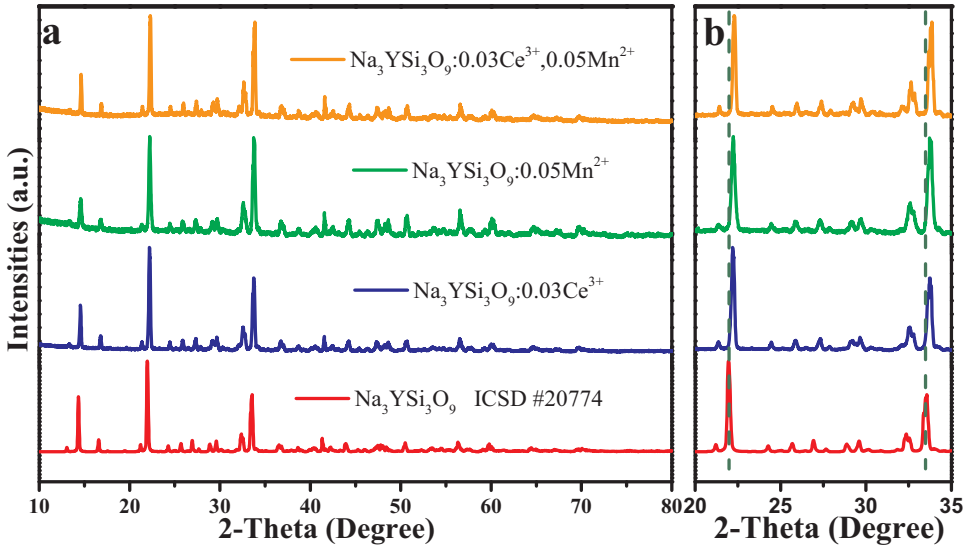

Fig. 1. (a) XRD patterns of NYS:0.03Ce^{3+}, NYS:0.05Mn^{2+} and NYS:0.03Ce^{3+}, 0.05Mn^{2+} with the standard pattern (ICSD #20774); (b) Detailed XRD pattern ranging from 20° to 35° of the same samples.

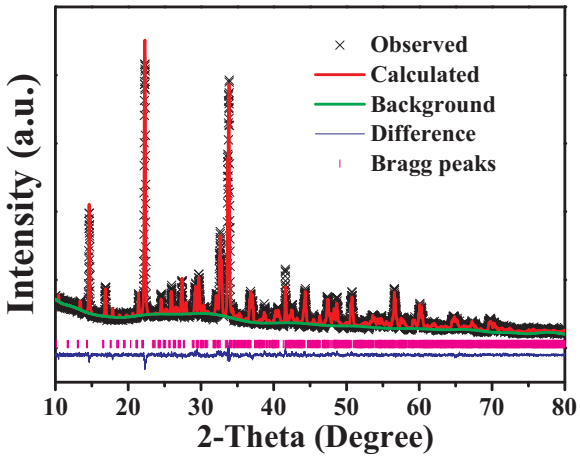

Fig. 2. Rietveld refinements for the XRD pattern of NYS:0.03Ce^{3+}, 0.05Mn^{2+}.

Table 1
Main parameters of NYS:0.03Ce^{3+}, 0.05Mn^{2+}.

Compound	NYS:0.03Ce^{3+}, 0.05Mn^{2+}
Symmetry	Orthorhombic
Space group	*P* 21 21 21
a (Å)	15.2138(8)
b (Å)	15.1452(4)
c (Å)	15.0363(1)
$\alpha = \beta = \gamma$ (deg.)	90
V (Å^3)	3464.63(8)
Z	16
2θ range (deg.)	10–80
R_{wp} %	6.44
R_p %	5.07
χ^2	1.948

x = 0.01–420 nm for x = 0.05 and the emissions of Mn^{2+} have almost no shift in NYS:xCe^{3+}, 0.05Mn^{2+}. When the concentration of Ce^{3+} or Mn^{2+} is increased, there is an obvious red shift associated with Ce^{3+} or Mn^{2+} while not the other one. The emission redshift is mainly caused by the chemical and physical changes of the host lattices, induced by the doping of Ce^{3+} and Mn^{2+}. It indicates that the doping ions changing only affect the lattice environment around the doping ion itself, and its influence on the other ions is very weak. Similar red shift

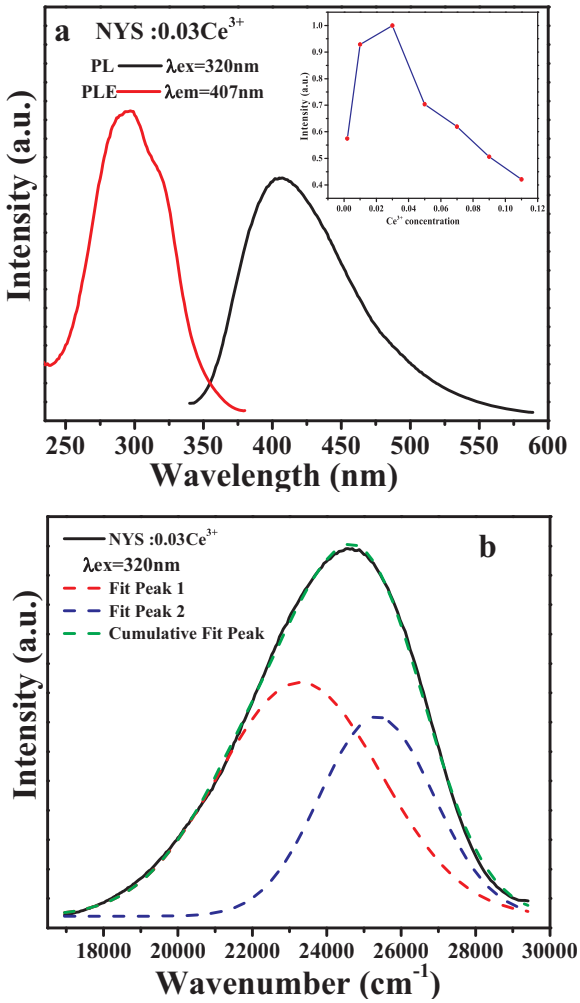

Fig. 3. (a) PL (λ_{ex} = 320 nm) and PLE (λ_{em} = 407 nm) spectra of NYS:0.03Ce^{3+}; the inset shows the variation of Ce^{3+} emission intensity as a function of the Ce^{3+} content; (b) PL spectrum of NYS:0.03Ce^{3+} and its Gaussian components.

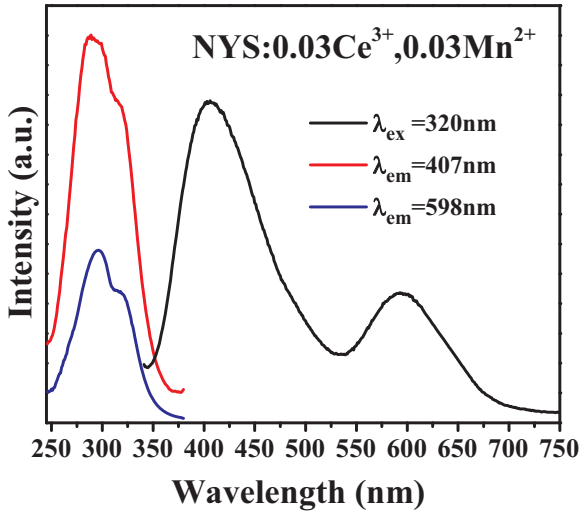

Fig. 4. PL (λ_{ex} = 320 nm) and PLE (λ_{em} = 407 nm and λ_{em} = 598 nm) spectra of NYS:0.03Ce^{3+}, 0.03Mn^{2+}.

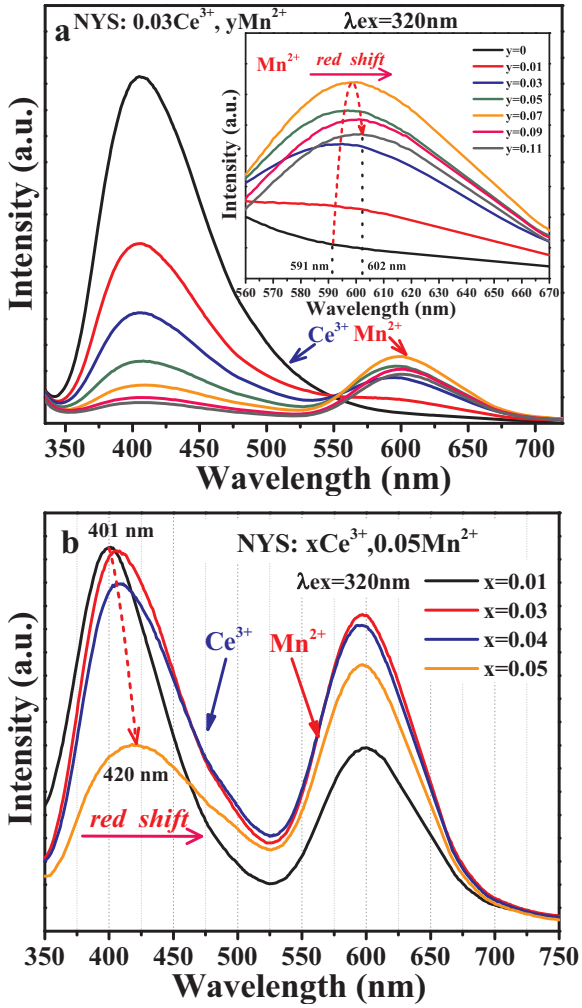

Fig. 5. (a) PL (λ_{ex} = 320 nm) spectra of NYS:0.03Ce^{3+}, yMn^{2+} (y = 0–0.11) and the inset shows the enlarged emission spectra in the range from 560 to 670 nm; (b) PL (λ_{ex} = 320 nm) spectra of NYS:xCe^{3+}, 0.05Mn^{2+} (y = 0.01–0.05).

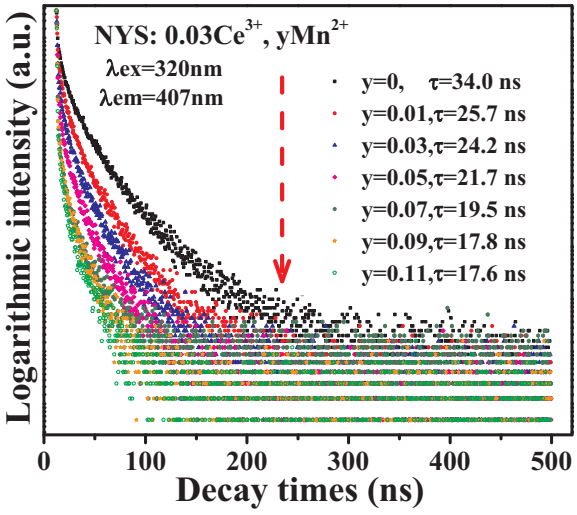

Fig. 6. Decay curves and lifetimes of the Ce^{3+} emission monitored at 407 nm in NYS:0.03Ce^{3+}, yMn^{2+} (y = 0–0.11) (λ_{ex} = 320 nm).

phenomenon of Ce^{3+} and Mn^{2+} has been also discussed in detail in the literature [31].

To further demonstrate the energy transfer from Ce^{3+} to Mn^{2+}, the fluorescence decay curves of Ce^{3+} monitored at 407 nm in NYS:0.03Ce^{3+}, yMn^{2+} (y = 0–0.11) were collected. As shown in Fig. 6, the decay of Ce^{3+} becomes faster and faster with increasing Mn^{2+} ions. All decay curves deviate from a single-exponential model, and are fitted by a double-exponential decay model as [28]:

$$I = A_1 exp(-t/\tau_1) + A_2 exp(-t/\tau_2) \quad (1)$$

where I is the luminescence intensity, A_1 and A_2 are constants, t is the time, and τ_1 and τ_2 are the short and long lifetimes for exponential components. And the average lifetime (τ) can be calculated by the following equation:

$$\tau = (A_1\tau_1^2 + A_1\tau_2^2)/(A_1\tau_1 + A_1\tau_2) \quad (2)$$

The average lifetimes (τ) of Ce^{3+} were calculated to be 34.0, 25.7, 24.2, 21.7, 19.5, 17.8 and 17.6 ns, corresponding to y = 0, 0.01, 0.03, 0.05, 0.07, 0.09 and 0.11. The decreased lifetimes of Ce^{3+} with increasing Mn^{2+} concentrations further confirm the energy transfer from Ce^{3+} to Mn^{2+}.

Generally, the energy transfer efficiency (η_T) from a sensitizer to an activator can be expressed by the following equation [32]:

$$\eta_T = 1 - \frac{I_s}{I_{so}} \quad (3)$$

where η_T is the energy transfer efficiency and I_{so} and I_S are the luminescence intensity of Ce^{3+} ions with the absence and presence of Mn^{2+} ions, respectively. Fig. 7 shows the energy transfer efficiency η_T and the relative emission intensity of Ce^{3+} ions as a function of Mn^{2+} content y for NYS:0.03Ce^{3+}, yMn^{2+}. More precisely, the η_T were determined to be 46.13%, 65.14%, 78.84%, 85.91%, 89.97% and 91.90% for y = 0.01, 0.03, 0.05, 0.07, 0.09, 0.11, respectively, indicating an efficient energy transfer from Ce^{3+} to Mn^{2+}. With increasing Mn^{2+} concentration, the relative emission intensity of Ce^{3+} decreased, while the energy transfer efficiency monotonously ascends as shown in Fig. 7. The transfer efficiency is gentle when the Mn^{2+} concentration is larger than 0.06 mol%. The reason could be concluded from two aspects—the fixed Ce^{3+} restricting the energy transfer and the quenching of Mn^{2+} [27].

Normally, the main mechanisms of the energy transfer include two types: exchange interaction and electric multipolar interaction. The critical distance between the sensitizer and activator for exchange interaction should be in the range of 5–8 Å [25]. The critical distance $R_{Ce\text{-}Mn}$ between Ce^{3+} to Mn^{2+}, for energy transfer has been calculated by

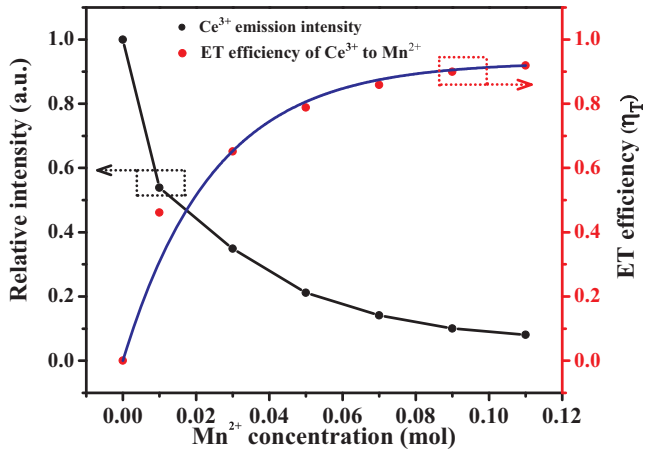

Fig. 7. Dependence of the Ce^{3+} emission and the energy transfer efficiency of Ce^{3+}-Mn^{2+} on the Mn^{2+} doping concentrations for NYS:0.03Ce^{3+}, yMn^{2+} (y = 0–0.11).

using the concentration quenching method, as suggested by Blasse [33]:

$$R_{Ce-Mn} \approx 2\left(\frac{3V}{4\pi x_c N}\right)^{\frac{1}{3}} \quad (4)$$

where V is the volume of the unit cell, x_c is the total concentration of Ce^{3+} and Mn^{2+} when the emission intensity of Ce^{3+} is half of that in the sample with the absence of Mn^{2+}, and N is the number of cations in the unit cell. In the present case, the values V = 3464.63 Å^3, x_c = 0.049, N = 64. Thus, the critical distance $R_{Ce\text{-}Mn}$ of energy transfer of NYS:0.03Ce^{3+}, yMn^{2+} was calculated to be 12.836 Å, which is longer than 5–8 Å. This indicates that the exchange interaction is not dominant, and the energy transfer from Ce^{3+} to Mn^{2+} may take place *via* multipolar interaction.

According to Dexter's energy transfer expression of multipolar interaction and Reisfeld's approximation, the following relation can be given as [34,35]:

$$\eta_0/\eta \propto C \text{ and } \eta_0/\eta \propto C^{n/3} \quad (5)$$

where η_0 and η are the luminescence quantum efficiencies of Ce^{3+} with the absence and presence of Mn^{2+}, respectively. C is the concentration of the sum of Ce^{3+} and Mn^{2+}. The relation of $\eta_0/\eta \propto C$ corresponds to the exchange interaction, while the relations of $\eta_0/\eta \propto C^{n/3}$ with n = 6, 8, or 10 corresponds to dipole-dipole, dipole–quadrupole, and quadrupole-quadrupole interactions, respectively. The value of η_0/η can be approximately estimated from the luminescence intensity ratio (I_{S0}/I_S) as follows:

$$I_{S0}/I_S \propto C \text{ and } I_{S0}/I_S \propto C^{n/3} \quad (6)$$

in which I_{S0} and I_S stand for the emission intensity of Ce^{3+} in the absence and presence of Mn^{2+}, respectively. The linear fits to the relationship between I_{S0}/I_S *versus* C as well as I_{S0}/I_S *versus* $C^{n/3}$ based on the above equation are illustrated in Fig. 8. The linear relationship reaches the optimal one for $I_{S0}/I_S \propto C^{6/3}$ by comparing the fitting

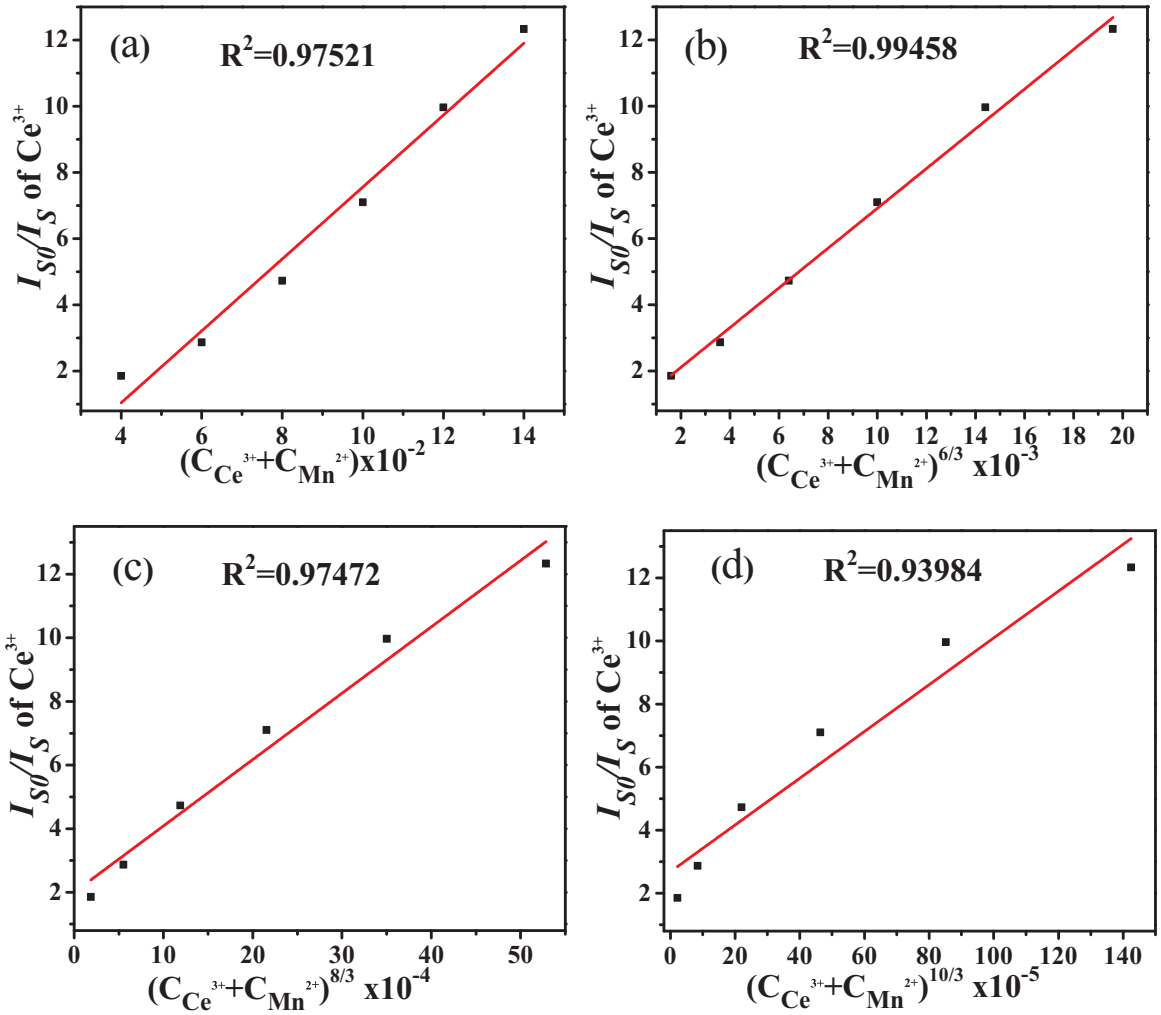

Fig. 8. Dependence of I_{S0}/I_S of Ce^{3+} on (a) C, (b) $C^{6/3}$, (c) $C^{8/3}$ and (d) $C^{10/3}$.

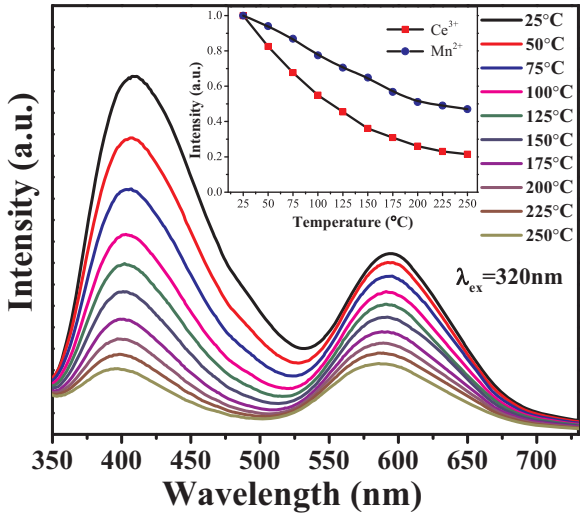

Fig. 9. Temperature-dependent PL spectra of NYS:0.03Ce^{3+}, 0.03Mn^{2+}; the inset shows the Ce^{3+} and Mn^{2+} emission intensity as a function of temperature excited at 320 nm.

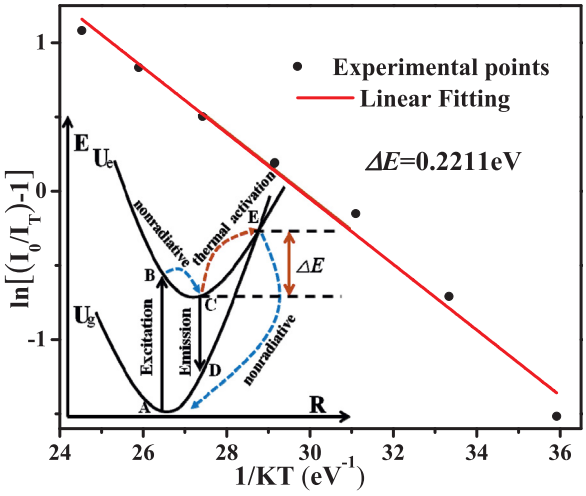

Fig. 10. Linear fitting of $ln[(I_0/I_t) - 1]$*versus* 1/KT for thermal quenching of NYS:0.03Ce^{3+}, 0.03Mn^{2+}; the inset shows the configuration coordinate diagram for the explanation of thermal quenching.

factors of R^2 values in Fig. 8, clearly indicating the dipole-dipole interaction between Ce^{3+} and Mn^{2+} in the NYS:0.03Ce^{3+}, yMn^{2+}.

3.4. Thermal quenching properties

The temperature-dependent emission spectra of the NYS:0.03Ce^{3+}, 0.03Mn^{2+} were depicted in Fig. 9. With temperature increasing from 25 °C to 250 °C, both the characteristic emission of Ce^{3+} and Mn^{2+} decrease gradually, and the thermal stability of Mn^{2+} is found to be better than that of Ce^{3+}. The emission intensity of Mn^{2+} decreases to 64.2% at 150 °C of that at 25 °C, while the value is 34.7% for Ce^{3+}, as shown in the inset in Fig. 9. The thermal quenching can be explained by a configurationally coordinate diagram. As temperature increases, the interaction of electron-phonon is intensive. More electrons in the excited state can be thermally activated to overcome the energy barrier Δ E and cross-over to the ground state. As a result, the nonradiative transition becomes more dominant. The nonradiative transition process is strongly dependent on the temperature and enhanced with the increases in temperature, resulting in the decreases of the emission intensity [36].

To further investigate the thermal quenching process, we calculated the activation energy (Δ*E*) from the Arrhenius equation [37]:

$$I_T = \frac{I_0}{1+cexp\,(-\Delta E/kT)} \quad (7)$$

where I_0 is the initial emission intensity, I_T is the intensity at different temperatures, *c* is a constant for a certain host, Δ*E* is the activation energy for thermal quenching and *k* is the Boltzmann constant (8.62×10^{-5} eV). According to the equation, the activation energy Δ*E* can be calculated by linear fitting the relationship of $ln\,[(I_0/I_T)-1]$ *versus* *1/kT*, and the straight slope is -Δ*E*. As shown in Fig. 10, the activation energy (Δ*E*) for thermal quenching was calculated to be 0.221 eV.

3.5. CIE chromaticity coordinates

The Commission International de L'Eclairage (CIE) chromaticity coordinates of NYS with different Ce^{3+} and Mn^{2+} contents excited at 320 nm are calculated and shown in Table 2 and Fig. 11. For NYS:0.03Ce^{3+}, yMn^{2+} (y = 0–0.11), the color tone can be tuned from blue (0.1701, 0.1101) to yellow (0.4499, 0.3441) as y increases from 0 to 0.11. NYS:xCe^{3+}, 0.05Mn^{2+} (x = 0.01–0.05) shows white light emission with a tunable color tone from (0.3533, 0.2404) to (0.3828, 0.3144) when the Ce^{3+} concentrations increase. The obtained white light owns a lower CCT from 2098 to 4866 K due to the abundant orange-red-emitting components. These results indicate that NYS:xCe^{3+}, yMn^{2+} can be modulated in a large color gamut and give wide-range warm-white-light emissions.

Table 2
CIE coordinates and CCT of NYS:xCe^{3+}, yMn^{2+} excited at 320 nm.

No.	NYS:xCe^{3+}, yMn^{2+}	CIE(*x*, *y*)	T_c
1	x = 0.03, y = 0	(0.1701,0.1101)	10,760 K
2	x = 0.03, y = 0.01	(0.2164,0.1685)	829,693 K
3	x = 0.03, y = 0.03	(0.2918,0.2293)	15,378 K
4	x = 0.03, y = 0.05	(0.3627,0.2855)	3612 K
5	x = 0.03, y = 0.07	(0.4192,0.3274)	2419 K
6	x = 0.03, y = 0.09	(0.4372,0.3378)	2215 K
7	x = 0.03, y = 0.11	(0.4499,0.3441)	2098 K
a	x = 0.01, y = 0.05	(0.3533,0.2404)	4866 K
b	x = 0.02, y = 0.05	(0.3589,0.2779)	3678 K
c	x = 0.04, y = 0.05	(0.3567,0.2835)	3892 K
d	x = 0.05, y = 0.05	(0.3828,0.3144)	3238 K

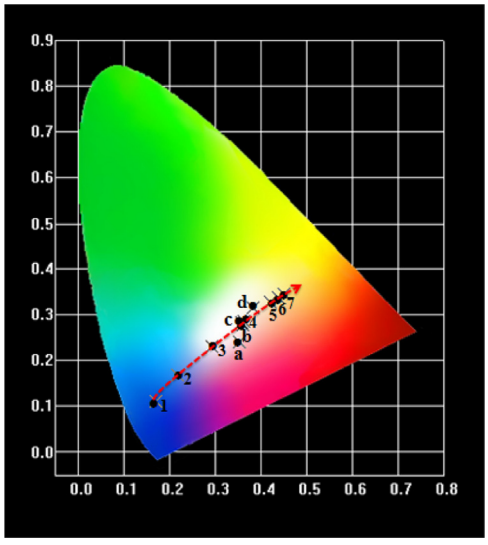

Fig. 11. CIE chromaticity diagram of NYS:0.03Ce^{3+}, yMn^{2+} (y = 0–0.11) and NYS:xCe^{3+}, 0.05Mn^{2+} (y = 0.01–0.05) excited at 320 nm.

4. Conclusion

In summary, samples of Ce^{3+} and Mn^{2+} activated NYS have been prepared by a conventional high-temperature solid-state reaction. The energy transfer from Ce^{3+} to Mn^{2+} in NYS:Ce^{3+}, Mn^{2+} was observed based on the luminescence spectra and fluorescence decay curves of Ce^{3+}. The resonance-type energy transfer was demonstrated to be a dipole-dipole interaction mechanism. The critical distance of energy transfer was calculated to be 12.836 Å and the maximum energy transfer efficiency was about 91.9%. The temperature dependence luminescence was investigated and the corresponding activation energy Δ E was calculated to be 0.221 eV. Utilizing the energy transfer from Ce^{3+} to Mn^{2+}, the emission color of NYS:Ce^{3+}, Mn^{2+} can be tuned from the blue region (0.1701, 0.1101) to yellow region (0.4499, 0.3441) by systematically adjusting the concentration ratio of Ce^{3+} and Mn^{2+}. Under NUV light excited, warm white light emissions with CIE = (0.3627, 0.2855) and CCT = 3612 K can be realized. All the results indicate that $Na_3YSi_3O_9$:Ce^{3+}, Mn^{2+} may have potential application for UV-pumped w-LEDs.

Acknowledgments

This work is financially supported by the National Key Research and Development Program of China (2016YFC0101803), the Natural Science Foundation Project of Chong Qing (cstc2017jcyjA0925), and the Public Projects of Zhejiang Province (LGG18E020007).

References

[1] Y. Liu, P. Liu, L. Wang, C. Cui, H. Jiang, J. Jiang, A two-step solid-state reaction to synthesize the yellow persistent $Gd_3Al_2Ga_3O_{12}$:Ce^{3+} phosphor with an enhanced optical performance for AC-LEDs, Chem. Commun. 53 (2017) 10636–10639.
[2] G. Li, Y. Tian, Y. Zhao, J. Lin, Recent progress in luminescence tuning of Ce^{3+} and Eu^{2+}-activated phosphors for pc-WLEDs, Chem. Soc. Rev. 44 (2015) 8688–8713.
[3] Z. Xia, Q. Liu, Progress in discovery and structural design of color conversion phosphors for LEDs, Prog. Mater. Sci. 84 (2016) 59–117.
[4] E.F. Schubert, J.K. Kim, Solid-state light sources getting smart, Science 308 (2005) 1274–1278.
[5] S. Tonzani, Lighting technology: time to change the bulb, Nature 459 (2009) 312–314.
[6] J. Li, J. Yan, D. Wen, W.U. Khan, J. Shi, M. Wu, Q. Su, P.A. Tanner, Advanced red phosphors for white light-emitting diodes, J. Mater. Chem. C 4 (2016) 8611–8623.
[7] S. Pimputkar, J.S. Speck, S.P. DenBaars, S. Nakamura, Prospects for LED lighting, Nat. Photonics 3 (2009) 180–182.
[8] V. Bachmann, C. Ronda, A. Meijerink, Temperature quenching of yellow Ce^{3+} luminescence in YAG:Ce, Chem. Mater. 21 (2009) 2077–2084.
[9] Y. Liu, J. Silver, R. Xie, J. Zhang, H. Xu, H. Shao, J. Jiang, H. Jiang, An excellent cyan-emitting orthosilicate phosphor for NUV-pumped white LED application, J. Mater. Chem. C 5 (2017) 12365–12377.
[10] K. Li, D. Geng, M. Shang, Y. Zhang, H. Lian, J. Lin, Color-tunable luminescence and energy transfer properties of $Ca_9Mg(PO_4)_6F_2$:Eu^{2+}, Mn^{2+} phosphors for UV-LEDs, J. Phys. Chem. C 118 (2014) 11026–11034.
[11] N. Guo, Y. Zheng, Y. Jia, H. Qiao, H. You, Warm-white-emitting from Eu^{2+}/Mn^{2+}-codoped $Sr_3Lu(PO_4)_3$ phosphor with tunable color tone and correlated color temperature, J. Phys. Chem. C 116 (2011) 1329–1334.
[12] C.-H. Huang, T.-S. Chan, W.-R. Liu, D.-Y. Wang, Y.-C. Chiu, Y.-T. Yeh, T.-M. Chen, Crystal structure of blue–white–yellow color-tunable $Ca_4Si_2O_7F_2$:Eu^{2+}, Mn^{2+} phosphor and investigation of color tunability through energy transfer for single-phase white-light near-ultraviolet LEDs, J. Mater. Chem. 22 (2012) 20210–20216.
[13] W.-J. Yang, L. Luo, T.-M. Chen, N.-S. Wang, Luminescence and energy transfer of Eu-and Mn-coactivated $CaAl_2Si_2O_8$ as a potential phosphor for white-light UVLED, Chem. Mater. 17 (2005) 3883–3888.
[14] Y. Song, G. Jia, M. Yang, Y. Huang, H. You, H. Zhang, $Sr_3Al_2O_5Cl_2$:Ce^{3+}, Eu^{2+}: a potential tunable yellow-to-white-emitting phosphor for ultraviolet light emitting diodes, Appl. Phys. Lett. 94 (2009) 091902.
[15] D. Geng, M. Shang, Y. Zhang, H. Lian, Z. Cheng, J. Lin, Tunable luminescence and energy transfer properties of $Ca_5(PO_4)_2SiO_4$:Ce^{3+}/Tb^{3+}/Mn^{2+} phosphors, J. Mater. Chem. C 1 (2013) 2345–2353.
[16] A. Huang, Z. Yang, C. Yu, Z. Chai, J. Qiu, Z. Song, Tunable and white light emission of a single-phased $Ba_2Y(BO_3)_2Cl$:Bi^{3+}, Eu^{3+} phosphor by energy transfer for ultraviolet converted white LEDs, J. Phys. Chem. C 121 (9) (2017) 5267–5276.
[17] J. Li, Q. Liang, J.Y. Hong, L. Dolgov, Y. Meng, Y. Xu, J. Shi, M. Wu, White light emission and enhanced color stability in a single-component host, ACS Appl. Mater. Interfaces 10 (2018) 18066–18072.
[18] Y. Xiao, Z. Hao, L. Liang, W. Xiao, D. Wu, X. Zhang, G. Pan, Y. Luo, J. Zhang, Highly efficient green-emitting phosphors $Ba_2Y_5B_5O_{17}$ with low thermal quenching due to fast energy transfer from Ce^{3+} to Tb^{3+}, Inorg. Chem. 56 (8) (2017) 4538–4544.
[19] W. Wang, Y. Yang, Y. Liu, D. Pan, X. Luo, S. Yan, G. Xiang, Y. Jin, Photoluminescence properties and efficient energy transfer of Ce^{3+}/Eu^{2+} activated $K_2Ba_7Si_{16}O_{40}$ phosphors, Mater. Res. Bull. 101 (2018) 232–239.
[20] Z. Lu, Z. Mao, J. Chen, D. Wang, Red/blue-shift dual-directional regulation of alpha-(Ca, Sr)$_2SiO_4$:Eu^{2+} phosphors resulting from the incorporation content of Eu^{2+}/Sr^{2+} ions, Dalton Trans. 44 (2015) 15620–15627.
[21] Y. Liu, J. Zhang, C. Zhang, J. Xu, G. Liu, J. Jiang, H. Jiang, $Ba_9Lu_2Si_6O_{24}$:Ce^{3+}: an efficient green phosphor with high thermal and radiation stability for solid-state lighting, Adv. Opt. Mater. 3 (8) (2015) 1096–1101.
[22] D. Ananias, L. Carlos, J. Rocha, Unusual full-colour phosphors: $Na_3LnSi_3O_9$, Opt. Mater. 28 (2006) 582–586.
[23] F. Wang, W. Wang, L. Zhang, J. Zheng, Y. Jin, J. Zhang, Luminescence properties and its red shift of blue-emitting phosphor $Na_3YSi_3O_9$:Ce^{3+} for UV LED, RSC Adv. 7 (2017) 27422–27430.
[24] B.H. Toby, EXPGUI, a graphical user interface for GSAS, J. Appl. Cryst. 34 (2001) 210–213.
[25] G. Blasse, B. Grabmaier, Energy Transfer. Chapter 5 in Luminescent Materials, Springer, 1994, pp. 91–107 https://www.springer.com/us/book/9783540580195.
[26] J. Chen, Y. Liu, L. Mei, Z. Wang, M. Fang, Z. Huang, Emission redshift and energy transfer behavior of color-tunable $KMg_4(PO_4)_3$:Eu^{2+}, Mn^{2+} phosphors, J. Mater. Chem. C 3 (2015) 5516–5523.
[27] W. Dai, Investigation of the luminescent properties of Ce^{3+} doped and Ce^{3+}/Mn^{2+} co-doped $CaAl_2Si_2O_8$ phosphors, RSC Adv. 4 (2014) 11206–11215.
[28] C.-H. Huang, P.-J. Wu, J.-F. Lee, T.-M. Chen, (Ca, Mg, Sr)$_9Y(PO_4)_7$:Eu^{2+}, Mn^{2+}: phosphors for white-light near-UV LEDs through crystal field tuning and energy transfer, J. Mater. Chem. 21 (2011) 10489–10495.
[29] J. Sun, Z. Lian, G. Shen, D. Shen, Blue–white–orange color-tunable luminescence of Ce^{3+}/Mn^{2+}-codoped $NaCaBO_3$ via energy transfer: potential single-phase white-light-emitting phosphors, RSC Adv. 3 (2013) 18395–18405.
[30] Y. Wang, H. Zhang, Q. Wei, C. Su, D. Zhang, Solid state synthesis, tunable luminescence and thermal stability of $NaCaBO_3$:Eu^{2+}/Mn^{2+} phosphors, Ceram. Int. 42 (10) (2016) 12422–12426.
[31] K. Park, J. Lee, J. Park, J. Kim, P. Kung, S.M. Kim, G. Kim, White-light generation through Ce^{3+}/Mn^{2+}-codoped and Eu^{2+}-doped $Ba_{1.2}Ca_{0.8}SiO_4$ T-phase phosphors, J. Lumin. 130 (2010) 2442–2445.
[32] H. Zhou, Y. Jin, M. Jiang, Q. Wang, X. Jiang, A single-phased tunable emission phosphor $MgY_2Si_3O_{10}$:Eu^{3+}, Bi^{3+} with efficient energy transfer for white LEDs, Dalton Trans. 44 (2015) 1102–1109.
[33] G. Blasse, Energy transfer in oxidic phosphors, Philips Res. Rep. 24 (1969) 131–144.
[34] D. Dexter, J.H. Schulman, Theory of concentration quenching in inorganic phosphors, J. Chem. Phys. 22 (1954) 1063–1070.
[35] R. Reisfeld, E. Greenberg, R. Velapoldi, B. Barnett, Luminescence quantum efficiency of Gd and Tb in borate glasses and the mechanism of energy transfer between them, J. Chem. Phys. 56 (1972) 1698–1705.
[36] J.Y. Han, W.B. Im, G. Lee, D.Y. Jeon, Near UV-pumped yellow-emitting Eu^{2+}-doped $Na_3K(Si_{1-x}Al_x)_8O_{16\pm\delta}$ phosphor for white-emitting LEDs, J. Mater. Chem. 22 (2012) 8793–8798.
[37] C.-H. Huang, T.-M. Chen, Novel yellow-emitting $Sr_8MgLn(PO_4)_7$:Eu^{2+} (Ln = Y, La) phosphors for applications in white LEDs with excellent color rendering index, Inorg. Chem. 50 (2011) 5725–5730.